Dalton Transactions

ROYAL SOCIETY OF CHEMISTRY

PAPER

View Article Online
View Journal | View Issue

Cite this: *Dalton Trans.*, 2025, **54**, 4267

Copper(III) organometallic complexes of non (anti) aromatic and aromatic doubly N-confused porphyrinoids: syntheses and characterization†

Anirban Panua,[a] Gunasekaran Velmurugan,[b] Peter Comba *[b] and Harapriya Rath *[a]

Received 22nd November 2024,
Accepted 25th January 2025

DOI: 10.1039/d4dt03265a

rsc.li/dalton

The retrosynthetic design and synthesis of three unprecedented doubly N-confused porphyrinoids with tunable aromaticity are reported. The controlled modification of the type of oxidant (chloranil *vs.* DDQ) led to the isolation of cross-conjugated doubly N-confused porphyrinoid **7** (upon chloranil oxidation) and Hückel aromatic porphyrinoid **8**, while DDQ oxidation led to the [16]π Hückel-antiaromatic porphyrinoid **9**. All three hybrid N-confused porphyrinoids **7–9** have been thoroughly characterized *via* solution-state spectroscopic measurements and in-depth DFT studies. While **7** and **8** could form respective Cu(III) organometallic complexes, porphyrinoid **9** remained unsusceptible to Cu metallation.

Introduction

The proton transfer tautomerism of porphyrins and their derivatives has been extensively researched owing to their biological significance and to understand the intriguing mechanism involved.[1] The four nitrogens at the core of porphyrins typically undergo rapid tautomerism, with each tautomer existing in equilibrium with comparable stability. In contrast, unique NH-tautomerism is very evident in the case of unsymmetrical porphyrinoids, such as corrole,[2] N-confused porphyrins,[3] and N-fused porphyrins.[4] The electronic structures and photophysical properties change significantly through NH-tautomerization. NH-tautomers usually exist in equilibrium and the tautomeric ratio is dependent on solvents, additives, temperature, and so on. Therefore, it is typically challenging to analyse or compare any NH-tautomer under comparable experimental settings. However, through *N*-alkylation, NH-tautomerization is intrinsically prevented and N-confused porphyrins[5] and doubly N-confused porphyrins[6] have been fixed as one type of tautomer.

The indigenous properties of π-conjugated macrocycles are mostly manifested in their molecular architecture and total number of π-electrons.[7] Aromaticity is one of the most fundamental concepts in chemistry that determines the structure, high stability and reactivity of molecules.[8] Within the premises of Hückel's rule, cyclic and planar conjugated molecules with 4n + 2 π-electrons are usually referred to as aromatic and stable, while cyclic and planar molecules with 4n π-electrons are referred to as antiaromatic and unstable.[9] The inherent destabilization of [4n]π-antiaromatic molecules[10] hinders synthetic chemists from conducting further chemical functionalization to explore their essential applications if any.[11] It must be emphasized that the antiaromatic destabilization in smaller [4n]π-systems (n = 1) is more significant than in larger 4n annulenes ($n \geq 2$).[12] In attempts to stabilize [16]π tetrapyrrolic porphyrins (Chart S1†),[13] the deformation of the conjugated core, and/or metalation and/or introduction of *meso*-alkyl groups have so far been the most adapted protocols found in the literature. In contrast, we report for the very first time the high-yield synthesis, and spectroscopic and solid-state structural proof of the lactam-embedded smallest-ever metal-free stable Hückel antiaromatic *trans*-doubly *N*-methyl N-confused [16]-porphyrins **IIIa**/**IIIb** (Chart 1).[6b] Intriguingly, these new

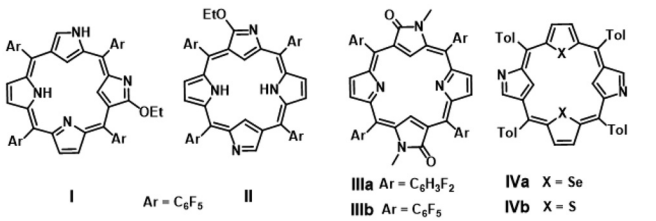

Chart 1 Progress in four-membered doubly N-confused porphyrinoids.

[a]*School of Chemical Sciences, Indian Association for the Cultivation of Science, 2A/2B Raja S.C Mullick Road, Jadavpur, Kolkata, West Bengal 700 032, India. E-mail: ichr@iacs.res.in*

[b]*Heidelberg University, Institute of Inorganic Chemistry and Interdisciplinary Center for Scientific Computing, Im Neuenheimer Feld 270, 69120 Heidelberg, Germany. E-mail: peter.comba@aci.uni-heidelberg.de*

†Electronic supplementary information (ESI) available. See DOI: https://doi.org/10.1039/d4dt03265a

facets of *trans*-doubly *N*-methyl N-confused porphyrins were susceptible to exhibiting the redox-associated variation of Hückel aromaticity as a mere consequence of the amido-like structures of the *N*-methyl N-confused pyrrole rings of the macrocycles.

It should be highlighted that the controlled modification of the basic framework of N-confused porphyrinoids results in unique optical and electronic properties that have no direct parallel in the chemistry of normal porphyrins. Thus, it is pertinent to the retrosynthetic design and synthesis of more and more structural analogues of *meso*-aryl-substituted doubly N-confused and/or N-fused porphyrinoids. Since the introduction of confusion into tetrapyrrolic macrocycles causes a significant loss of thermodynamic stability,[14] only a handful of reports (Chart 1) are available in the field of doubly N-confused tetrapyrrolic porphyrins,[6,15] where either two N-confused pyrrole rings or two *N*-methyl N-confused pyrrole rings are introduced into the macrocyclic core. This has served as an incentive for an in-depth study exploring the NH-tautomerism, π-conjugation and aromaticity/antiaromaticity in tetrapyrrolic doubly N-confused porphyrins upon introducing an *N*-methyl N-confused pyrrole and an N-confused pyrrole ring into the macrocycle core. These results are discussed herein.

Results and discussion

Given the focus of our present study, we adopted [3 + 1] acid-catalysed conventional oxidative condensation of *N*-methyl N-confused tripyrrane **4** and N-confused pyrrole dicarbinol **6**, using *p*-toluene sulfonic acid (*p*-TSA), followed by oxidation using 2.5 equivalents of chloranil, as outlined in Scheme 1.[6a] With this reaction strategy, we anticipated the isolation of cross-conjugated non-aromatic doubly N-confused porphyrin **7** as a minor product and doubly N-confused porphyrin **8** as the major product. Column chromatographic separation over basic alumina, followed by repeated silica gel (200–400 mesh) chromatographic separation and preparative thin layer chromatography (PTLC) techniques, led to the isolation of air-stable **7** in 5% yield as a brown solid and **8** in 15% yield as a green solid. In contrast, under the same reaction conditions, using DDQ as oxidant, we observed the formation of doubly N-confused porphyrinoid **9** in 17% yield as a green solid. The compositions of **7–9** were confirmed by positive-mode ESI-TOF mass spectrometry, which showed the parent ion peak at *m*/*z* 774.1951 calc. for $C_{45}H_{25}F_8N_4$ $[M + H]^+$ corresponding to macrocycle **7** (Fig. S1†), at *m*/*z* 789.1901 calc. for $C_{45}H_{25}F_8N_4O$ $[M + H]^+$ for macrocycle **8** (Fig. S2†) and at *m*/*z* 803.1771 calc. for $C_{45}H_{23}F_8N_4O_2$ $[M + H]^+$ for macrocycle **9** (Fig. S3†). The presence of the C=O group was confirmed by a band at 1706 cm^{-1} for **8** (Fig. S7†) and at 1697 cm^{-1} for **9** in the IR spectrum (Fig. S8†).

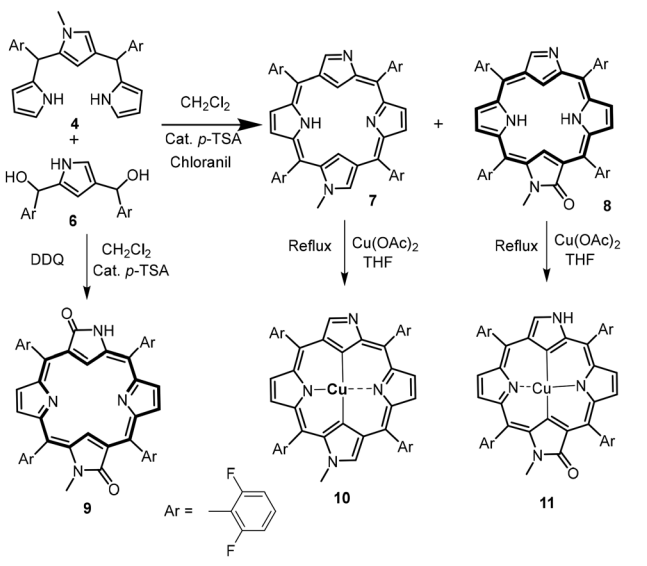

Scheme 1 Rational syntheses of doubly N-confused porphyrinoids **7–9** and copper(III) complexes **10**, **11**.

UV-vis and NMR spectroscopic analysis of 7–9

A solution of **7** in CH_2Cl_2 exhibits a green colour (Fig. 1A) with the electronic absorption spectrum comprising a split Soret band at 454 and 524 nm and an ill-defined Q-type band at 600 nm, stretching up to 800 nm, indicating the lack of efficient π-conjugation, typical of non-aromatic porphyrinoids.[16] Solutions of **8** in CH_2Cl_2 exhibit a green colour (Fig. 1B) with the electronic absorption spectrum comprising a sharp Soret band at 438 nm, one Q-type band at 652 nm and another Q-type band at 717 nm stretching up to 800 nm, indicating efficient π-conjugation, typical of aromatic porphyrinoids.[6a,16] On a similar note, a solution of **9** in CH_2Cl_2 exhibits a green colour (Fig. 1C) with the electronic absorption spectrum comprising a Soret band at 475 nm and a broad Q-type band at 599 nm and another broad band at 1066 nm stretching up to 1200 nm, similar to *trans*-doubly *N*-methyl N-confused antiaromatic porphyrinoids.[6a] All these spectral patterns of macrocycle **9** indicate efficient π-conjugation, typical of anti-aromatic porphyrinoids.[16] In conjunction with the electronic absorption spectral patterns, the ^{1}H NMR spectroscopic analysis of **7** in $CDCl_3$ strongly supports the lack of cyclic π-conjugated structures, with the observation of an NH signal in the low-field region and the appearance of CH signals of heterocyclic rings in the alkenic region, typifying nonaromaticity. For macrocycle **7**, a well-resolved spectral pattern, assignable to all the protons in the macrocycle, has been achieved at ambient temperature. The individual peak assignments of **7**, as shown in Fig. S22,† based on 2D COSY, ROESY, HSQC and HBMC spectra (Fig. S17–S21†), reveal doublets at δ = 6.15 ppm and 5.81 ppm as the β-CH protons (*a*, *b*), doublets at δ = 6.10 ppm and 5.74 ppm as the β-CH protons (*c*, *d*), and broad signals at δ = 5.75 ppm and 6.84 ppm as the α-CH protons (*e*, *f*), while the signals at δ = 6.24 ppm and 6.19 ppm have been assigned to the β-CH protons (*g*, *h*), and the 3H signal at 3.77 ppm as the methyl peak of the *N*-methyl N-confused pyrrole ring. The observations of disrupted π-conjugation, owing to cross-conjugation, are thus very

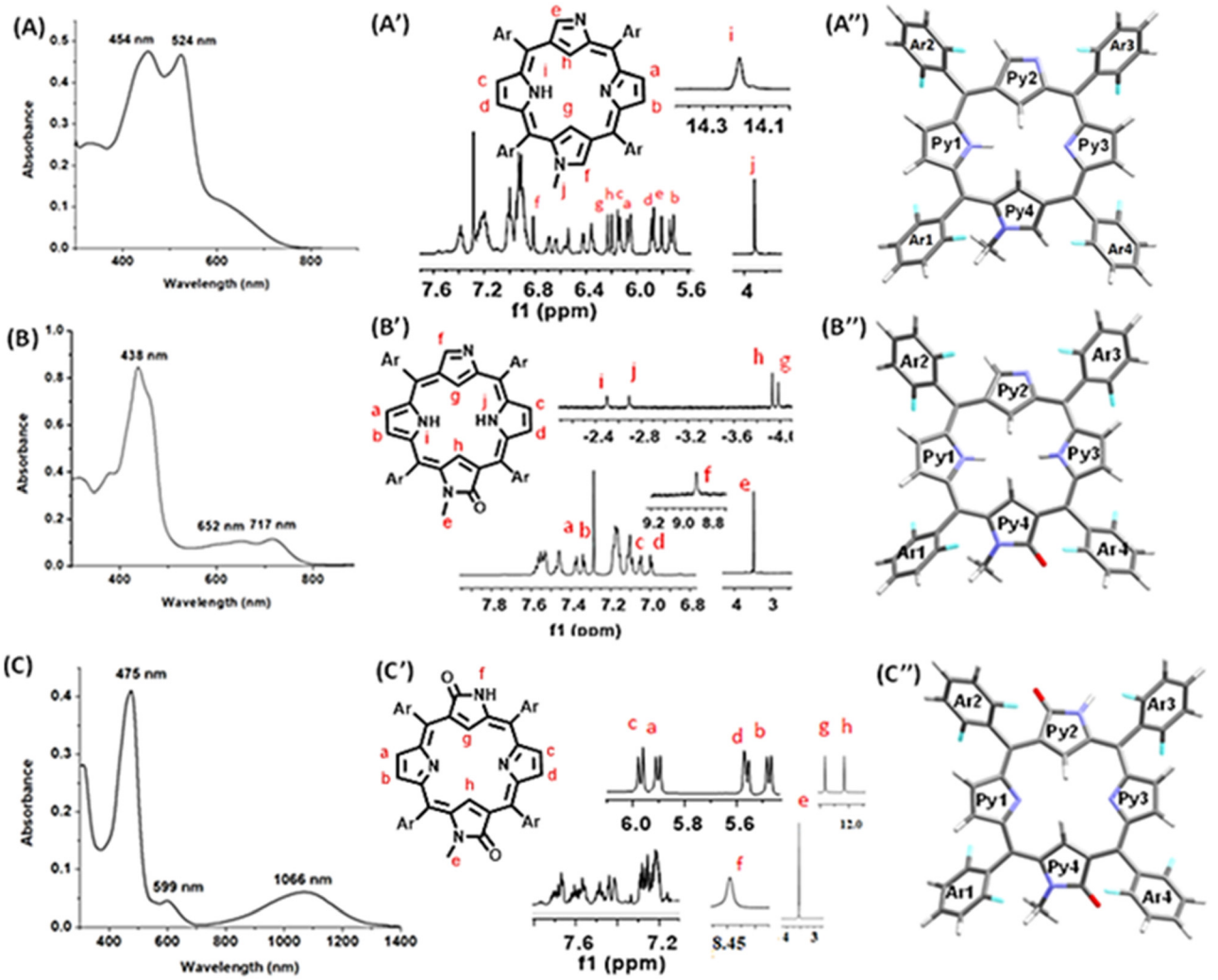

Fig. 1 UV-vis absorption spectra of (A) **7**, (B) **8** and (C) **9** as the free base in CH_2Cl_2 at 298 K; completely assigned ^1H NMR spectra of (A′) **7**, (B′) **8** and (C′) **9** as the free base in CD_2Cl_2 at 298 K; DFT optimised geometries of **7** (A″), **8** (B″) and **9** (C″).

evident. It is worth mentioning that cross-conjugation effects have lately been recognized as having an impact on molecular conductance resonances[17] and electron transfer rates,[18] and this type of structural motif has been extensively studied in annulene chemistry.[19] On a similar note, the individual peak assignments of **8**, as shown in Fig. S29,† based on 2D COSY, ROESY, HSQC and HBMC spectra (Fig. S23–S28†), reveal doublets at δ = 7.37 ppm and 7.34 ppm as the β-CH protons (*a*, *b*), doublets at *d* = 7.05 ppm and 7.01 ppm as the β-CH protons (*c*, *d*), and the broad signals at δ = 8.90 ppm as the α-CH protons (*e*), while the signals at δ = −3.91 ppm and −3.96 ppm have been assigned to the inner β-CH protons (*g*, *h*), the signals at δ = −2.37 ppm and −2.59 ppm to the inner NH protons (*i*, *j*), and the 3H signal at 3.46 ppm as the methyl peak of the *N*-methyl N-confused pyrrole ring. These observations revealed a sustained diatropic ring current ($\Delta\delta$ = 12.86 ppm)[20] in macrocycle **8**, in line with its electronic absorption spectra. Similarly, the individual peak assignments of **9**, as shown in Fig. S36,† based on 2D COSY, ROESY, HSQC and HBMC spectra (Fig. S31–S35†), reveal doublets at δ = 5.92 ppm and 5.53 ppm as the β-CH protons (*a*, *b*), and doublets at δ = 5.98 ppm and 5.55 ppm as the β-CH protons (*c*, *d*), while the signals at δ 12.45 ppm and 12.14 ppm have been assigned to the inner β-CH protons (*g*, *h*), the signals at δ 8.44 ppm to the inner NH protons (*f*), and the 3H signal at 3.51 ppm as the methyl peak of the *N*-methyl N-confused pyrrole ring. Based on these premises, **9** is attributed to exhibiting [16]π antiaromatic nature.[21] The observed weak antiaromaticity of **9** is in line with the weaker shielding/deshielding influence anticipated in most *N*-substituted N-confused porphyrinoids reported to date.[5d,e,6,22]

DFT studies of 7–9

For macrocycles **7**–**9**, the lack of suitable single crystals for X-ray diffraction analysis necessitated the use of geometric optimisation based on density functional theory (DFT). The optimisations were performed at the B3LYP/6-31G(d,p) level of theory.[23] Scheme S2† summarizes all possible isomers and

tautomers of **7–9**.[14] The NH tautomers (**7** and **7′**) and isomers (**7″** and **7‴**) show structural similarity, with an energy difference within 8.14 kJ mol^{-1} (Fig. S50, 51 and Table S1†). Also **8** and **8′** are nearly isoenergetic with a difference of 0.57 kJ mol^{-1}. However, compound **9** is significantly more stable than **9′** with an energy difference of 22.85 kJ mol^{-1}. The C–C (1.376–1.431 Å) and C–N (1.304–1.403 Å) bond lengths in compound **8** (Fig. S48†) fall within the range of single and double bonds, indicating enhanced π-electron delocalization across the macrocycle. The amino-type pyrrole and keto groups on the *N*-methyl N-confused pyrrole in **8** facilitate greater delocalisation compared to **7**. On the other hand, the imine-type pyrrole in **7** suppresses delocalisation, as reflected in the slightly longer C–C bond lengths compared to **8** (Fig. S47 and S48†). The orientation of the *meso*-aryl groups influences the dihedral angles in the macrocycles. The angles between the $(C_{meso})_4$ plane and the *meso*-aryl groups range from 48.14° to 66.34° in **7–9**. The amino/imine-type pyrrole rings exhibit smaller dihedral angles (Py1: 10.46°–21.33°; Py3: 10.84°–19.66°) compared to the N-confused pyrrole ring (Py2: 14.25°–21.35°; Py4: 24.29°–27.01°). The perpendicular orientation of the *meso*-aryl rings to the macrocyclic plane contributes to the overall planarity of the macrocycles. In **8**, the planarity is enhanced compared to **7** due to the amino-type pyrrole Py1 and keto group on the *N*-methyl N-confused pyrrole Py4. However, compound **9** exhibits significantly reduced planarity compared to **8**, due to the presence of an additional keto group on the N-confused pyrrole ring Py2 and the imine-type pyrrole Py1 (Table S2†). The HOMO levels of compounds **7–9** are progressively destabilized, with the energy levels of −4.48 eV (**7**), −4.90 eV (**8**), and −5.24 eV (**9**), reflecting a decrease of 0.42 and 0.76 eV, respectively. Similarly, the LUMO levels are destabilised with energy values of −2.74 eV (**7**), −2.53 eV (**8**), and 3.31 eV (**9**). The HOMO–LUMO gap is smallest for **7** (1.74 eV), followed by **9** (1.93 eV), and then **8** (2.37 eV) (Fig. 2 and S60†). In porphyrinoid **7**, the HOMO is primarily localised on the amino/imine-type pyrrole rings (17.93% at Py1 and 4.42% at Py3) and the N-confused pyrrole groups (13.60% at Py2 and 12.02% at Py4). Significant contributions to the HOMO also come from the *meso*-aryl groups between the amino-type and N-confused pyrrole rings (20.12% at Ar1 and 18.45% at Ar2). The LUMO electron cloud is distributed mainly between the imine-type pyrrole and N-confused pyrrole rings (12.58% at Ar3, 18.79% at Ar4, 18.34% at Py2, 12.84% at Py3 and 17.31% at Py4). Contributions from *meso*-aryl groups and pyrrole rings are notable in HOMO−1, HOMO−2, LUMO+1, and LUMO+2. However, HOMO−2 is predominantly localised on the imine-type pyrrole (39.72%) and N-confused pyrrole (33.07%), while LUMO+3 is largely localised on the *meso*-aryl group Ar1 (74.36%). In porphyrinoid **8**, the keto group on the *N*-methyl N-confused pyrrole Py4 and the amino-type pyrrole Py3 induce changes in aryl-group contributions. Specifically, the HOMO contributions are 11.08% at Ar2, 10.57% at Ar3, 16.76% at Ar4, 12.88% at Py3, and 18.40% at Py4, while the LUMO contributions are 15.20% at Ar1, 18.46% at Ar3, 16.47% at Py3, and 17.34% at Py4. In the case of **9**, the electron cloud distribution shows that the pyrrole rings contribute more than 61% to the HOMO and 66% to the LUMO, significantly exceeding the contribution from aryl groups (Tables S3–S5 and Fig. S62†). Time-dependent density functional theory (TD-DFT) calculations[24] were conducted to investigate the electronic transitions in the doubly N-confused porphyrinoids (Fig. S80–S82 and Tables S11–S13†). For **7**, the Soret band at 431 nm and the Q-band at 588 nm (extending up to 797 nm) correspond to the transitions HOMO−2 → LUMO (83%) and HOMO → LUMO (97%), respectively. Porphyrinoid **8** shows a Soret band at 456 nm and a Q-band at 689 nm, associated with the transitions HOMO−1 → LUMO (55%), HOMO → LUMO+1 (22%), HOMO−1 → LUMO+1 (11%), and HOMO → LUMO (78%), HOMO−1 → LUMO+1 (21%), respectively. For **9**, the Soret band at 486 nm corresponds to the HOMO−3 → LUMO transition (84%), aligning well with experimental observations, whereas the broad NIR band (attributed to transitions from HOMO → LUMO orbitals (100%), Fig. S82 and Table S13†) seems to be underestimated.

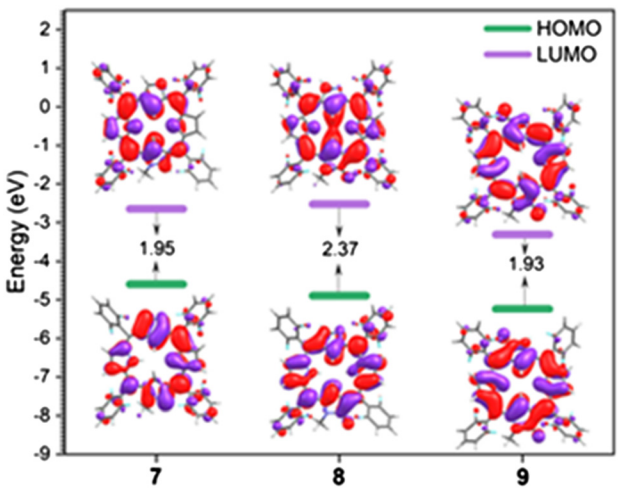

Fig. 2 FMO energy levels of doubly N-confused porphyrinoids **7–9**.

To understand the aromaticity of these macrocycles, the anisotropy of the induced current density (ACID) plots[25] and contour maps of the localised orbital locator (LOL) topology were analysed.[26] The AICD plot (Fig. S65†) of porphyrinoid **7** displays a clockwise ring current, which is interrupted at the N-confused pyrrole and imine pyrrole of the macrocyclic core, favouring the nonaromatic character of compound **7**. In **8**, distinct diatropic (clockwise) ring currents along the macrocyclic conjugation pathway confirm its aromatic nature (Fig. 3a). However, paratropic (anti-clockwise) ring currents in porphyrinoid **9** reveal its anti-aromatic character (Fig. S67†). Localised π-electron density and electron localisation function (ELF) maps[26] further confirm interrupted conjugation in **7** and strong macrocyclic conjugation in **8**. The Wiberg bond index (WBI)[27] decomposition for **8** (1.01–1.68) supports π-electron delocalisation along the macrocycle, with contributions from C–C and C–N bonds. The existence of a larger macrocyclic con-

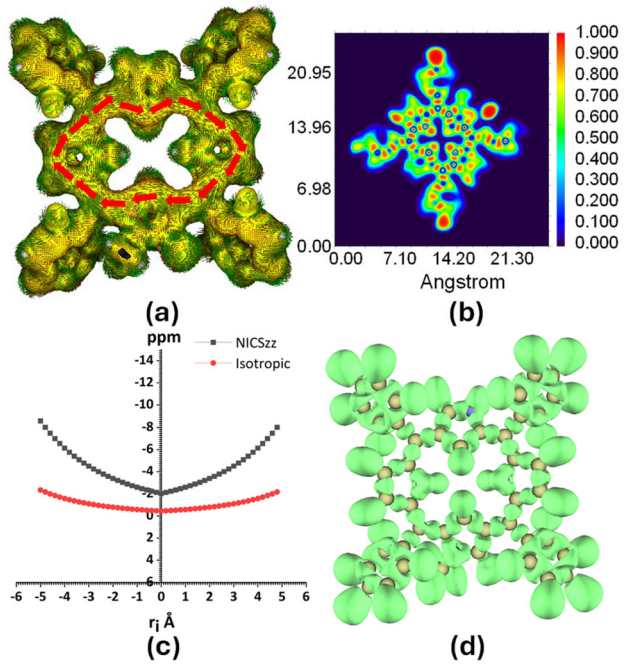

Fig. 3 (a) The anisotropy of induced current density (AICD) plot of **8**. A continuous clockwise ring current along the macrocycle indicates the aromatic nature of the macrocycle. (b) A contour map of the π-localized orbital locator of **8**. (c) Isotropic NICS and NICSzz scan plots of **8**, where NICSzz is the out-of-plane contribution. (d) Computed ELF index of **8**.

jugation in **8** is supported by the computed multi-centre index value (MCI)[28] (0.576). The harmonic oscillator model of aromaticity values (HOMA),[29] computed along the π-conjugation pathway are 0.804 (**8**) and 0.421 (**9**), respectively (Table S9†). The higher HOMA value of **8** confirms its strong aromatic nature and the low HOMA value of the porphyrinoid **9** indicates anti-aromaticity. The ELF indices (Fig. S74–S76†), computed at bifurcation points, indicate better electron localisation and bonding in **8** compared to **9**, where reduced localisation signifies weaker interaction between ELF domains. The aromaticity indices AV1245 and AVmin also corroborate these findings. The large difference between AV1245 and AVmin shows interrupted conjugation in **7**, which confirms its non-aromatic nature. Porphyrinoid **8** shows higher AV1245 values, indicating stronger delocalisation along the macrocyclic pathway, compared to the individual rings, while lower AV1245 and AVmin values in **9** suggest poor macrocyclic conjugation (Table S19†). Nucleus-independent chemical shift (NICS)[30] calculations further elucidate the aromaticity of these macrocycles. In **8**, NICS (0) = −11.239 and NICS (1) = −11.359, with NICS scan curves showing negative values up to 5.0 Å above and below the plane, confirming aromaticity (Fig. 3).

For **9**, NICS (0) = 7.927 and NICS (1) = 6.686, with NICS scan curves exhibiting positive values at similar distances, consistent with anti-aromaticity (Fig. S78†). These results strongly support the non-aromatic, aromatic and anti-aromatic nature of porphyrinoids **7**, **8** and **9**, respectively.

Cu metalation of 7–9

The organometallic chemistry of copper is almost entirely centred on the metal oxidation state +1, while classical coordination chemistry is dominated by the $Cu^{I/II}$ couple, with Cu^{III} often observed as a reactive intermediate in catalytic cycles.[31] Electron-rich organocopper(I) compounds are commonly used as reagents in a variety of organic syntheses.[32] Organocopper (III) transient species were considered in the mechanism of multiple bond activation *via* a reactive π-complex. Their transformation into σ-carbon–copper(III) intermediates[33] was followed by reductive elimination. Depending on whether the two outer pyrrole nitrogens are of amine or imine type, the doubly N-confused porphyrin (N_2CP) can serve as an $N_2(CH)_2$, an $N(NH)(CH)_2$, or an $(NH)_2(CH)_2$ ligand.[34] A handful of reports are available of Cu-doubly N-confused tetrapyrrolic porphyrinoids (Chart 2).[35] This has sparked the idea of unravelling the ability of all three doubly N-confused porphyrinoids **7–9** to stabilize Cu(II)/Cu(III), the details of which are described in the following section.

Under mild conditions in an inert atmosphere, using anhydrous THF, macrocycle **7**/**8** was stirred under reflux with Cu $(CH_3COO)_2$ for 1–8 h. Subsequently, the solvent was removed and hexane was added to extract a red residue that precipitated after solvent volume reduction. The residue was then purified by silica gel column chromatography and recrystallised from DCM–hexane solution to obtain the uncharged Cu^{III} complex **10**/**11** in 80–84% yield (Scheme 1). HR-ESI-TOF MS (positive mode) of **10** yielded a mass peak with m/z = 832.0933, in line with the calculated mass of 832.0934 for $C_{45}H_{21}CuF_8N_4$ $[M]^+$ (Fig. S4†). HR-ESI-TOF MS (positive mode) of **11** yielded a mass peak with m/z = 848.0883, in line with the calculated mass of 848.0884 for $C_{45}H_{21}CuF_8N_4O$ $[M]^+$ (Fig. S5†). The UV/vis absorption spectrum of **10** (Fig. 2A) in CH_2Cl_2 reveals a strong transition at 455 nm and a shoulder at 425 nm without any Q-type bands. In contrast, the UV/vis absorption spectrum of **11** (Fig. 2B) in CH_2Cl_2 reveals a strong transition at 339 nm and comparatively weak transitions at 456 nm, and well-defined Q type bands at 535 nm and 728 nm, in line with published data of other similar Cu^{III} complexes.[35]

The copper species **10** and **11** are EPR silent, suggesting that the Cu oxidation state is either Cu^{1+} (d^{10}) or Cu^{3+} (d^8). This is supported by distinct ^1H NMR signals in $CDCl_3$ in the range of 7.67 to 2.8 ppm (Fig. 4A′ and B′). NMR spectroscopy was very useful for deciphering the electronic structure of copper complex **10**/**11**. In **10**, the three inner protons are dissociated to create a well-preorganised trianionic ligand structure. Cross-peaks reveal pairwise coupling among four downfield pyrrole resonances at 7.54, 7.05 and between 7.27 and 7.0 ppm in the COSY spectrum (Fig. S37†). In the ROESY spectrum (Fig. S38†) the 3H singlet at 2.76 ppm, exhibiting a cross peak with the singlet at 6.82 ppm, strongly reveals the former as a methyl peak of the *N*-methyl N-confused pyrrole ring, and the latter as the signal of the α-CH of the same pyrrole ring. The singlet at 6.52 ppm has been unequivocally assigned as the signal of the α-CH of the N-confused pyrrole ring due to the

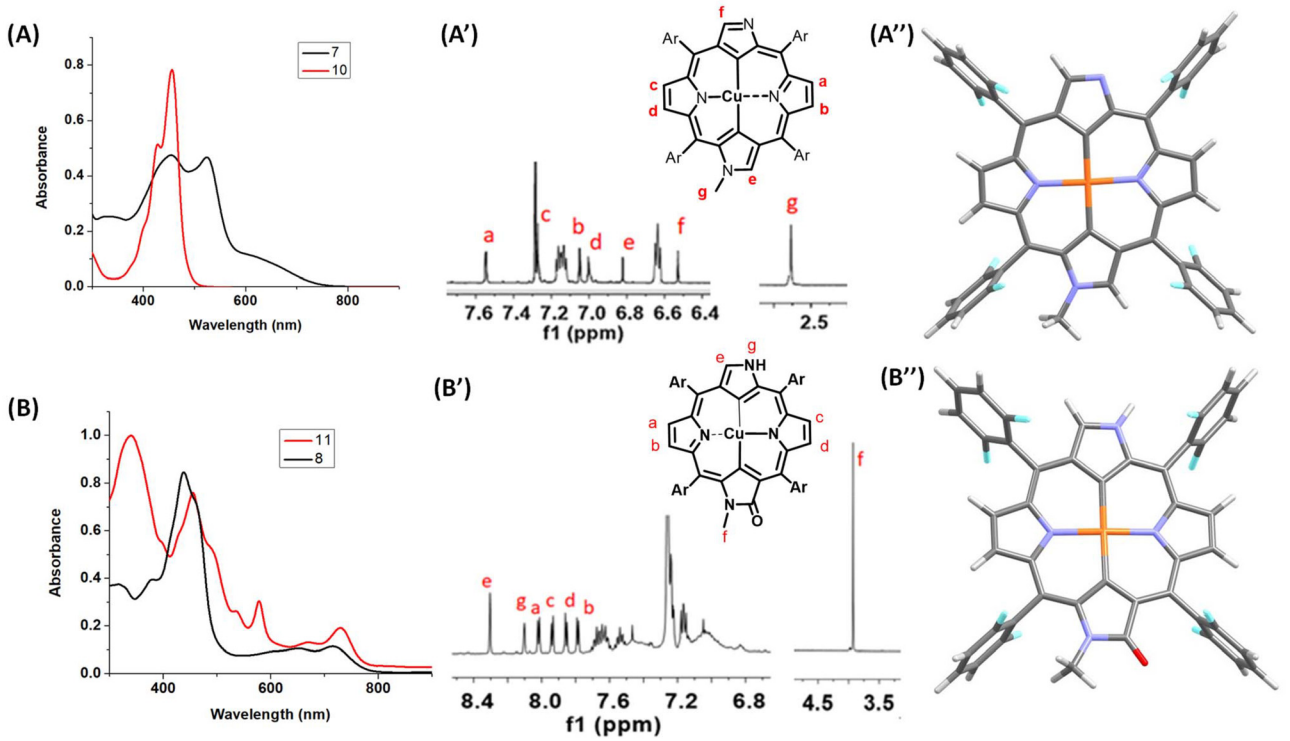

Fig. 4 UV-vis absorption spectra of **10** (A), and **11** (B) in CH_2Cl_2 at 298 K; completely assigned ^{1}H NMR spectra of **10** (A′), and **11** (B′) in $CDCl_3$ at 298 K; DFT-optimised geometries of **10** (A″), and **11** (B″).

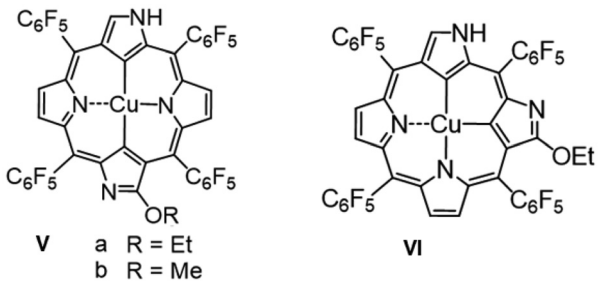

Chart 2 Cu-doubly N-confused porphyrinoids relevant to this work found in the literature.[35]

lack of any correlation between the 2D COSY and ROESY spectra. The ^{1}H NMR spectral pattern reveals no resonances ascribable to inner NH and the two inner –CH, suggesting **10** is a Cu^{III} complex, and this also follows from the stoichiometry of the uncharged complex and the fact that the complex has a singlet ground state. In **11**, out of four inner protons of ligand **8**, three inner protons are dissociated to create a well-pre-organised trianionic ligand structure, while one of the inner NH is transformed to an imine N at the expense of making the outer imine N of the N-confused pyrrole of ligand **8** into amine-type NH. This chameleon-like nature is well known in NCP-type macrocycles.[5] Cross-peaks reveal pairwise coupling among four downfield pyrrole resonances at 8.1, 7.7 ppm, and between 7.9, and 7.99 ppm in the COSY spectrum (Fig. S40†). As expected, no cross-peak is seen for the methyl resonance at 3.92 ppm, which can be assigned to the 3-H methyl peak of the *N*-methyl N-confused pyrrole. In the ROESY spectrum (Fig. S41†), the broad peak at 8.02 ppm, exhibiting a cross peak with the singlet at 8.1 ppm, strongly reveals the former as an NH peak of the N-confused pyrrole ring, and the latter as the signal of the α-CH of the same pyrrole ring. The ^{1}H NMR spectral pattern reveals no resonances ascribable to inner NH and the two inner –CH, suggesting that **11** is a Cu^{III} complex, and this also follows from the stoichiometry of the uncharged complex and the fact that the complex has a singlet ground state.

DFT studies of 10 and 11

To investigate the structural and electronic properties of macrocyclic ligand complexes **10** and **11**, we performed DFT and TD-DFT calculations.[23,24] The optimized geometries of **10** and **11** exhibit highly planar structures due to Cu metalation (Fig. S54–S57†).

In **10**, the Cu–N bond lengths range from 2.000 to 2.022 Å, while the Cu–C bond lengths are between 1.945 and 1.962 Å. Similarly, in **11**, the Cu–N bond lengths range from 2.006 to 2.016 Å, and the Cu–C bond lengths vary from 1.959 to 1.968 Å. The singlet spin states of **10** and **11** are energetically more stable than their triplet spin states, with stabilization energies of 17.88 kJ mol^{-1} for **10** and 12.73 kJ mol^{-1} for **11**. The spin density plots for **10** and **11** reveal spin polarisation between the Cu atom and the coordinated ligand. The spin

density of Cu is calculated to be 0.558 for **10** and 0.550 for **11**. For the pyrrole N atoms, the spin densities range from 0.169 to 0.207 in **10** and from 0.151 to 0.233 in **11**. The N-confused pyrrole C atoms exhibit spin densities between 0.333 and 0.494 in **10** and between 0.356 and 0.440 in **11**. The HOMO energy levels are calculated as −4.756 eV for **10** and −4.830 eV for **11**, while the LUMO energy levels are −2.852 eV for **10** and −2.928 eV for **11**, resulting in a HOMO–LUMO gap of 1.90 eV for both macrocycles (Tables S6 and S7†). In both **10** and **11**, the HOMO is delocalized across the macrocycle, with contributions of 10–14% from each *meso*-aryl group and 9–11% from each pyrrole ring, and a minor contribution from the Cu atom (6.04–6.64%). The LUMO, however, is primarily localized on the Cu atom (30–31%) and pyrrole rings (64%). The HOMO−1 and HOMO−2 are also mainly localised on the pyrrole rings (40% for HOMO−1, 23% for HOMO−2) and the N-confused pyrrole rings (50% for HOMO−1, 64% for HOMO−2). The LUMO+1 and LUMO+2 are localised on the pyrrole rings (>22% for LUMO+1, >33% for LUMO+2) and the coordinated *N*-methyl N-confused pyrrole (>43% for LUMO+1, >16% for LUMO+2). Interestingly, HOMO−3 is predominantly localised on the N-confused pyrrole (62%) and its adjacent *meso*-aryl group (Ar3, 24%), while the *meso*-aryl groups mainly contribute to LUMO+3. To account for the nature of the electronic transitions of **10** and **11** (Fig. S83 and S84†), TD-DFT calculations were performed. The results reveal that the strong transition at 454 nm and shoulder at 433 nm for **10** correspond to the electronic transitions HOMO−5 → LUMO (51%), HOMO−6 → LUMO (22%), HOMO−4 → LUMO (10%), and HOMO−5 → LUMO (40%), HOMO−6 → LUMO (39%), HOMO−3 → LUMO (12%), respectively (Table S13†). For macrocyclic ligand complex **11**, the transitions at 340 nm, 460 nm and the Q-bands are assigned to the transitions HOMO−14 → LUMO (29%), HOMO−13 → LUMO (18%), and HOMO−6 → LUMO (32%), HOMO−5 → LUMO (31%), HOMO−4 → LUMO (30%), and HOMO → LUMO+1 (100%), respectively (Fig. 5).

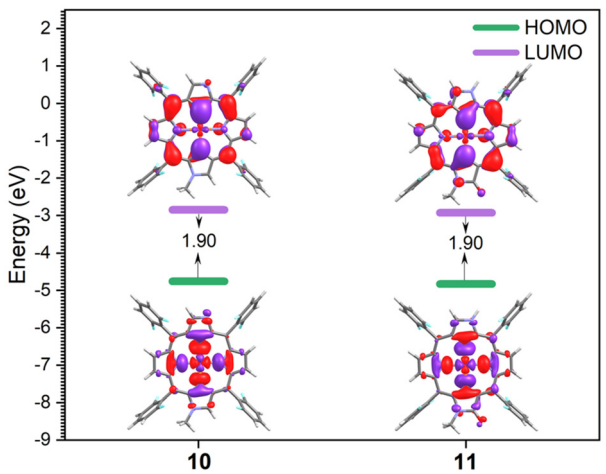

Fig. 5 FMO energy levels of copper(III) complexes **10–11**.

Electrochemistry of 7–11

The electrochemical properties of the new macrocycles and copper complexes were investigated with cyclic voltammetry in dichloromethane, using 0.01 M tetrabutylammonium hexafluorophosphate as supporting electrolyte. Two reversible oxidation waves at 0.77 V and 0.97 V and a quasireversible reduction peak at *ca.* −1.13 V yielded an estimate for the electrochemical HOMO–LUMO gap (HLG) of 1.99 V (Fig. S44†) for macrocycle **7**. For **8**, there are three irreversible oxidation peaks (0.61 V, 1.19 V and 1.43 V), one reversible oxidation peak (0.91 V), two irreversible reduction peaks (−0.69 V and 0.89 V) and one reversible reduction peak (−1.43 V) with a HOMO–LUMO energy gap of 1.30 V (Fig. S45†). The smaller HOMO–LUMO energy gap of **8** compared to its cross-conjugated non-aromatic counterpart **7**, indicates enhanced π-conjugation in the macrocycle with aromaticity. For macrocycle **9**, two reversible oxidation waves at 0.46 V and 0.89 V and two reversible reduction peaks at *ca.* −0.58 V and −0.85 V yielded an estimate of the electrochemical HOMO–LUMO gap (HLG) of 1.04 V (Fig. S46†). For copper complexes **10** and **11**, electrochemical studies could not be performed due to their low solubility in any organic solvent. The experimental HLG values for **7–9** are in line with DFT findings.

Conclusions

In conclusion, we have reported N-confused pyrrole and *N*-methyl N-confused pyrrole incorporated doubly N-confused porphyrinoids, displaying nonaromaticity, aromaticity, and anti-aromaticity, *via* selective oxidation, depending upon the type of oxidant used. On the basis of spectral studies supported by DFT, it has been concluded that the modified N-confused porphyrinoid **7** is cross-conjugated and hence non-aromatic, **8** is highly aromatic, while **9** is antiaromatic.

The electronic properties and structural details were further explored through DFT and TD-DFT calculations, which provided insights into the nature of the macrocyclic conjugation pathways. The HOMO and LUMO energy levels, frontier molecular orbital distributions, and narrow HOMO–LUMO gaps substantiate these findings. The non-aromatic nature of **7** is strongly supported by the interrupted clockwise ring current at the N-confused pyrrole and imine pyrrole of the macrocyclic core. The aromatic nature of **8** is supported by its distinct diatropic ring currents, high HOMA index (0.804), and multicenter index (MCI) values, along with the electron localization function (ELF) analyses. Conversely, the antiaromatic character of **9** is confirmed by paratropic ring currents, low HOMA values (0.421), and positive NICS values, supported by AV1245 and AVmin indices. Interestingly, while both **7** and **8** can form stable organometallic Cu(III) complexes (**10** and **11**), the anti-aromatic ligand **9** does not undergo Cu complexation, highlighting the influence of electronic structure on reactivity. DFT and TD-DFT studies of **10** and **11** reveal planar geometries stabilized by Cu metalation, with significant spin density polarization between the Cu center and the ligand.

Author contributions

HR designed the complete scientific project. AP synthesized all the macrocycles, purified the macrocycles and plotted all spectroscopic data. GV and PC implemented all theoretical data mentioned in the manuscript. HR and PC wrote the scientific content of the manuscript.

Data availability

The data underpinning this scientific investigation are available in the manuscript and its ESI.†

Conflicts of interest

There are no conflicts to declare.

Acknowledgements

This work is dedicated to Professor Vadapalli Chandrasekhar on the occasion of his 65th birthday. A. P. thanks CSIR, New Delhi, India, for a senior research fellowship, H. R. thanks SERB (SPG/2021/002173) New Delhi, India for a research grant. The theoretical study was conducted within the Max Planck School Matter to Life, supported by the German Federal Ministry of Education and Research (BMBF) in collaboration with the Max Planck Society and Heidelberg University. The authors acknowledge support by the state of Baden-Württemberg through bwHPC and the German Research Foundation (DFG) through grant no INST 40/575-1 FUGG (JUSTUS 2 cluster).

References

1 D. K. Maity, R. L. Bell and T. N. Truong, *J. Am. Chem. Soc.*, 2000, **122**, 897–906 and references therein.
2 (*a*) T. Ding, E. A. Alemán, D. A. Modarelli and C. J. Ziegler, *J. Phys. Chem. A*, 2005, **109**, 7411; (*b*) T. Ding, J. D. Harvey and C. J. Ziegler, *J. Porphyrins Phthalocyanines*, 2005, **9**, 22.
3 (*a*) M. Toganoh and H. Furuta, *Chem. Rev.*, 2022, **122**(9), 8313–8437; and references therein; (*b*) L. Latos-Grażyński, in *Porphyrin Handbook*, Academic Press, San Diego, 2000, vol. 2M.
4 M. Toganoh and H. Furuta, *Chem. Lett.*, 2019, **48**, 615–622; and references therein.
5 (*a*) M. Toganoh, T. Yamamoto, T. Hihara, H. Akimaru and H. Furuta, *Org. Biomol. Chem.*, 2012, **10**, 4367–4374; (*b*) N. Halder, M. Sangeetha, D. Usharani and H. Rath, *Org. Biomol. Chem.*, 2019, **17**, 6131–6135; (*c*) N. Halder, L. U. Dzhemileva, I. R. Ramazanov, V. A. D'Yakonov, U. M. Dzhemilev and H. Rath, *ChemMedChem*, 2020, **15**, 632–642; (*d*) N. Halder, K. C. Sahoo, K. Gourav, D. Usharani and H. Rath, *J. Org. Chem.*, 2021, **86**, 8015–8026; (*e*) M. Jana, G. Velmurugan, P. Comba and H. Rath, *Org. Chem. Front.*, 2024, **11**, 5077–5085.
6 (*a*) N. Halder, M. Sangeetha, D. Usharani and H. Rath, *J. Org. Chem.*, 2020, **85**, 2059–2067; (*b*) N. Halder, R. Narayanasami, D. Usharani and H. Rath, *Org. Chem. Front.*, 2022, **9**, 2333–2342.
7 M. Iyoda, J. Yamakawa and M. J. Rahman, Conjugated macrocycles: concepts and applications, *Angew. Chem., Int. Ed.*, 2011, **50**, 10522–10553.
8 (*a*) V. I. Minkin, M. N. Glukhovtsev and B. Y. Simkin, *Aromaticity and Antiaromaticity. Electronic and Structural Aspects*, John Wiley and Sons, New York, 1994; (*b*) P. v. R. Schleyer, *Chem. Rev.*, 2001, **101**, 1115–1118; (*c*) P. v. R. Schleyer, *Chem. Rev.*, 2005, **105**, 3433–3435; (*d*) A. Stanger, *Chem. Commun.*, 2009, 1939–1947; (*e*) N. Martin, M. M. Haley and R. Tykwinski, *Chem. Commun.*, 2012, **48**, 10471–10471; (*f*) R. Gleiter and G. Haberhauer, *Aromaticity and Other Conjugation Effects*, Wiley-VCH, Weinheim, Germany, 2012.
9 E. Z. Hückel, *Z. Phys.*, 1931, **70**, 204–286.
10 R. Breslow, *Acc. Chem. Res.*, 1973, **6**, 393–398.
11 (*a*) T. Nishinaga, T. Ohmae and M. Iyoda, *Symmetry*, 2010, **2**, 76–97; (*b*) B. K. Reddy, A. Basavarajappa, M. D. Ambhore and V. G. Anand, *Chem. Rev.*, 2017, **117**, 3420–3443; (*c*) Y. Tobe, *Top. Curr. Chem.*, 2018, **376**, 12–62; (*d*) Y. Sun, Y. Guo and Y. Liu, *Mater. Sci. Eng.*, 2019, **136**, 13–26.
12 C. S. Wannere, D. Moran, N. L. Allinger, B. A. Hess, L. J. Schaad and P. v. R. Schleyer, *Org. Lett.*, 2003, **5**, 2983–2986.
13 (*a*) Y. Yamamoto, A. Yamamoto, S. Furuta, M. Horie, M. Kodama, W. Sato, K. Akiba, S. Tsuzuki, T. Uchimaru, D. Hashizume and F. Iwasaki, *J. Am. Chem. Soc.*, 2005, **127**, 14540–14541; (*b*) J. A. Cissel, T. P. Vaid and G. P. A. Yap, *Org. Lett.*, 2006, **8**, 2401–2404; (*c*) Y. Yamamoto, Y. Hirata, M. Kodama, T. Yamaguchi, S. Matsukawa, K. Akiba, D. Hashizume, F. Iwasaki, A. Muranaka, M. Uchiyama, P. Chen, K. M. Kadish and N. Kobayashi, *J. Am. Chem. Soc.*, 2010, **132**, 12627–12638; (*d*) T. Kakui, S. Sugawara, Y. Hirata, S. Kojima and Y. Yamamoto, *Chem. – Eur. J.*, 2011, **17**, 7768–7771; (*e*) S. Sugawara, Y. Hirata, S. Kojima, Y. Yamamoto, E. Miyazaki, K. Takimiya, S. Matsukawa, D. Hashizume, J. Mack, N. Kobayashi, Z. Fu, K. M. Kadish, Y. M. Sung, K. S. Kim and D. Kim, *Chem. – Eur. J.*, 2012, **18**, 3566–3581; (*f*) T. Ito, Y. Hayashi, S. Shimizu, J.-Y. Shin, N. Kobayashi and H. Shinokubo, *Angew. Chem., Int. Ed.*, 2012, **51**, 8542–8545; (*g*) T. Yonezawa, S. A. Shafie, S. S. Hiroto and H. Shinokubo, *Angew. Chem., Int. Ed.*, 2017, **56**, 11822–11825; (*h*) F. Luo, L. Liu, H. Wu, L. Xu, Y. Rao, M. Zhou, A. Osuka and J. Song, *Nat. Commun.*, 2023, **14**, 5028.
14 H. Furuta, H. Maeda and A. Osuka, *J. Org. Chem.*, 2001, **66**, 8563–8572.
15 (*a*) H. Furuta, H. Maeda and A. Osuka, *J. Am. Chem. Soc.*, 2000, **122**, 803–807; (*b*) H. Maeda, Y. Ishikawa, T. Matsuda, A. Osuka and H. Furuta, *J. Am. Chem. Soc.*, 2003, **125**, 11822–11823; (*c*) H. Maeda, A. Osuka and H. Furuta, *J. Am. Chem. Soc.*, 2003, **125**, 15690–15691; (*d*) H. Furuta,

H. Maeda and A. Osuka, *J. Org. Chem.*, 2000, **65**, 4222–4226; (*e*) S. Sahoo, M. Sangeetha, S. Bera, D. Usharani and H. Rath, *Org. Biomol. Chem.*, 2020, **18**, 6058–6062.
16 M. Gouterman, *J. Mol. Spectrosc.*, 1963, **11**, 108–127.
17 (*a*) K. Shikama, *Chem. Rev.*, 1998, **98**, 1357–1373; (*b*) K. A. Magnus, H. Ton-That and J. E. Carpenter, *Chem. Rev.*, 1994, **94**, 727–735.
18 W. Wu and C. K. Chang, *J. Am. Chem. Soc.*, 1987, **109**, 3149–3150.
19 (*a*) V. Promarak and P. L. Burn, *J. Chem. Soc., Perkin Trans. 1*, 2001, 14–20; (*b*) C. K. Chang and W. Wu, *J. Biol. Chem.*, 1986, **261**, 8593–8596.
20 B. Frank and A. Nunn, *Angew. Chem., Int. Ed. Engl.*, 1995, **34**, 1795–1811.
21 J. A. Pople and K. G. Untch, *J. Am. Chem. Soc.*, 1966, **88**, 4811–4815.
22 (*a*) J. L. Sessler, D.-G. Cho, M. Stępień, V. Lynch, J. Waluk, Z. S. Yoon and D. Kim, *J. Am. Chem. Soc.*, 2006, **128**, 12640–12641; (*b*) P. J. Chmielewski and L. Latos-Grażyński, *J. Chem. Soc., Perkin Trans. 2*, 1995, 503–509.
23 (*a*) M. J. Frisch, G. W. Trucks, H. B. Schlegel, G. E. Scuseria, M. A. Robb, J. R. Cheeseman, G. Scalmani, V. Barone, G. A. Petersson, H. Nakatsuji, X. Li, M. Caricato, A. V. Marenich, J. Bloino, B. G. Janesko, R. Gomperts, B. Mennucci, H. P. Hratchian, J. V. Ortiz, A. F. Izmaylov, J. L. Sonnenberg, D. Williams-Young, F. Ding, F. Lipparini, F. Egidi, J. Goings, B. Peng, A. Petrone, T. Henderson, D. Ranasinghe, V. G. Zakrzewski, J. Gao, N. Rega, G. Zheng, W. Liang, M. Hada, M. Ehara, K. Toyota, R. Fukuda, J. Hasegawa, M. Ishida, T. Nakajima, Y. Honda, O. Kitao, H. Nakai, T. Vreven, K. Throssell, J. A. Montgomery Jr., J. E. Peralta, F. Ogliaro, M. J. Bearpark, J. J. Heyd, E. N. Brothers, K. N. Kudin, V. N. Staroverov, T. A. Keith, R. Kobayashi, J. Normand, K. Raghavachari, A. P. Rendell, J. C. Burant, S. S. Iyengar, J. Tomasi, M. Cossi, J. M. Millam, M. Klene, C. Adamo, R. Cammi, J. W. Ochterski, R. L. Martin, K. Morokuma, O. Farkas, J. B. Foresman and D. J. Fox, *Gaussian 16 Rev. C.01*, Wallingford, CT, 2016; (*b*) A. D. Becke, Density-Functional Thermochemistry III. The Role of Exact Exchange, *J. Chem. Phys.*, 1993, **98**, 5648–5652; (*c*) J. P. Perdew, *Phys. Rev. B: Condens. Matter Mater. Phys.*, 1986, **33**, 8822–8824; (*d*) A. D. Becke, *Phys. Rev. A*, 1988, **38**, 3098–3100; (*e*) C. Lee, W. Yang and R. G. Parr, *Phys. Rev. B:Condens. Matter Mater. Phys.*, 1988, **37**, 785–789; (*f*) P. J. Hay and W. R. Wadt, *J. Chem. Phys.*, 1985, **82**, 270; (*g*) W. R. Wadt and P. J. Hay, *J. Chem. Phys.*, 1985, **82**, 284; (*h*) P. J. Hay and W. R. Wadt, *J. Chem. Phys.*, 1985, **82**, 299.
24 (*a*) E. Runge and E. K. U. Gross, *Phys. Rev. Lett.*, 1984, **52**, 997–1000; (*b*) R. E. Stratmann, G. E. Scuseria and M. J. Frisch, *J. Chem. Phys.*, 1998, **109**, 8218–8224; (*c*) R. Bauernschmitt and R. Ahlrichs, *Chem. Phys. Lett.*, 1996, **256**, 454–464.
25 D. Geuenich, K. Hess, F. Köhler and R. Herges, *Chem. Rev.*, 2005, **105**, 3758–3772.
26 T. Lu and F. Chen, *J. Comput. Chem.*, 2012, **33**, 580–592.
27 (*a*) F. Weinhold, *J. Comput. Chem.*, 2012, **33**, 2363–2379; (*b*) E. D. Glendening, C. R. Landis and F. Weinhold, *J. Comput. Chem.*, 2013, **34**, 1429–1437.
28 P. Bultinck, R. Ponec and S. Van Damme, *J. Phys. Org. Chem.*, 2005, **18**, 706–718.
29 (*a*) T. M. Krygowski, *J. Chem. Inf., Comput. Sci.*, 1993, **33**, 77–78; (*b*) T. M. Krygowski and K. M. Cryański, *Chem. Rev.*, 2001, **101**, 1385–1420.
30 P. V. R. Schleyer, C. Maerker, A. Dransfeld, H. Jiao and N. J. R. v. E. Hommea, *J. Am. Chem. Soc.*, 1996, **118**, 6317–6318.
31 G. van Koten, S. L. James and J. T. B. H. Jastrzebski, in *Comprehensive Organometallic Chemistry II*, ed. E. W. Abel, F. G. A. Stone and G. Wilkinson, Elsevier Science Ltd, London, 1995, vol. 3.
32 *Organocopper Reagents: A Practical Approach*, ed. R. J. K. Taylor, Oxford University Press, UK, 1994.
33 (*a*) N. Krause and A. Gerold, *Angew. Chem., Int. Ed. Engl.*, 1997, **36**, 186–204; (*b*) E. Nakamura, S. Mori and K. Morokuma, *J. Am. Chem. Soc.*, 1997, **119**, 4900–4910; (*c*) R. F. de la Pradilla, M. B. Rubio, J. P. Marino and A. Viso, *Tetrahedron Lett.*, 1992, **33**, 4985–4988; (*d*) Y. Chounan, T. Ibuka and Y. Yamamoto, *J. Chem. Commun.*, 1994, 2003–2004.
34 (*a*) H. Furuta, H. Maeda and A. Osuka, *J. Am. Chem. Soc.*, 2000, **122**, 803–807; (*b*) K. Araki, H. Winnischofer, H. E. Toma, H. Maeda, A. Osuka and H. Furuta, *Inorg. Chem.*, 2001, **40**, 2020–2025; (*c*) H. Maeda, A. Osuka and H. Furuta, *Supramol. Chem.*, 2003, **15**, 447–450; (*d*) H. Furuta, H. Maeda and A. Osuka, *J. Org. Chem.*, 2000, **65**, 4222–4226; (*e*) H. Furuta, H. Maeda and A. Osuka, *J. Org. Chem.*, 2001, **66**, 8563–8572.
35 (*a*) H. Maeda, A. Osuka and H. Furuta, *J. Am. Chem. Soc.*, 2003, **125**, 15690–15691; (*b*) H. Furuta, H. Maeda, A. Osuka, M. Yasutake, T. Shinmyozu and Y. Ishikawa, *Chem. Commun.*, 2000, 1143–1144.